An Unsymmetric FDTD Subgridding Algorithm With Unconditional Stability

Jin Yan, *Member, IEEE*, and Dan Jiao, *Fellow, IEEE*

***Abstract*— To preserve accuracy in a grid with arbitrary subgrids, a finite-difference time-domain (FDTD) subgridding scheme, in general, would result in an unsymmetric numerical system. Such a numerical system can have complex-valued eigenvalues, which will render a traditional explicit time marching of FDTD absolutely unstable. In this paper, we develop an accurate FDTD subgridding algorithm suitable for arbitrary subgridding settings with arbitrary contrast ratios between the normal grid and the subgrid. Although the resulting system matrix is also unsymmetric, we develop a time-marching method to overcome the stability problem without sacrificing the matrix-free merit of the original FDTD. This method is general, which is also applicable to other subgridding algorithms whose underlying numerical systems are unsymmetric. The proposed FDTD subgridding algorithm is then further made unconditionally stable, thus permitting the use of a time step independent of space step. Extensive numerical experiments involving both 2- and 3-D subgrids with various contrast ratios have demonstrated the accuracy, stability, and efficiency of the proposed subgridding algorithm.**

***Index Terms*— Fast methods, finite-difference time-domain (FDTD) method, stability, subgridding, unconditionally stable methods.**

I. Introduction

THE finite-difference time-domain (FDTD) method is one of the most popular time-domain methods for electromagnetic analysis [1], [2]. This is mainly because of its simplicity and optimal computational complexity at each time step. The conventional FDTD method requires a uniform orthogonal grid. If there exist fine features in a structure, a fine space step must be used to discretize them. Because of the connected nature of an orthogonal grid, the regions where there are no fine features are also discretized in a smaller space step. This unnecessarily increases the number of unknowns to be solved. Subgridding is an effective means to address this problem, where fine grids are only placed in the necessary regions, which need not to be conformal to the background regular grid.

In an FDTD subgridding method, the fields at the interface between coarse and fine grids are typically estimated through certain interpolation scheme. Such an interpolation may ruin the positive semidefiniteness of the original FDTD numerical system, thereby causing instability. Meanwhile, the numerical reflections at the interface between coarse and fine grids and the different numerical dispersion in the two grids may result in a worse solution accuracy. Therefore, a good FDTD subgridding algorithm should guarantee both stability and accuracy.

In the literature, an extensive work has been done to tackle the FDTD subgridding problem. In [3], an initial run is made on a coarse grid, the result of which is then used as the boundary condition for a second calculation where the grid in the region of interest is refined. Later, a variable step-size method was developed in [4]. It provides a direct interpolation scheme to update fields in both coarse and fine grids simultaneously when a grid contrast ratio is 2. It also develops an interpolation scheme based on the wave equation for a contrast ratio of 3. The wave-equation-based scheme was improved to be a mesh refinement algorithm in [5] by interpolating a second-order difference at each mesh node, and later extended to be a multigrid displacement method by adding a buffer zone between coarse and fine meshes in [6]. To handle material traverse, a new subgridding algorithm in [7] was developed for odd contrast ratios. Later, a multigrid current method was proposed in [8] to handle any contrast ratio by using a weighted current value from the coarse region at the mesh interface to update the fine-region tangential fields on the same interface. To minimize the numerical reflection, Okoniewski *et al.* [9] proposed a new arrangement of mesh where the coarse and fine mesh are offset in all directions. Such a mesh allows the development of a pulsing overlapping scheme where the outermost layer of the fine mesh is dropped during update, but the mesh is expanded back to its original size at the end of each update cycle. Instability, especially late-time instability, has been observed in many of the aforementioned subgridding algorithms. Various approaches have been proposed to remedy this issue [6]–[9]. However, they still lack a theoretical study on the stability. In [10], a subgridding scheme with a reciprocal interpolation scheme was developed in a recessed subgridding interface with stability guaranteed, but the solution accuracy is compromised.

In [11] and [12], a class of subgridding algorithms was developed in the framework of the finite integration technique and the stability of this method is controlled by maintaining the consistency of the field coupling scheme. It has handled cases where the contrast ratio is 2. Another subgridding method based on the finite element method was proposed in [13]. The concept of maintaining the consistency of the field coupling scheme can also be found in [14], which is based on an equivalent passive network method. All of these methods involve hybridization with other methods.

Manuscript received August 29, 2017; revised March 4, 2018; accepted April 25, 2018. Date of publication May 11, 2018; date of current version August 2, 2018. This work was supported in part by a grant from NSF under Award 1619062 and in part by a grant from DARPA under Award HR0011-14-1-0057. *(Corresponding author: Dan Jiao.)*

J. Yan is with the Platform Engineering Group, Intel Corporation, Hillsboro, OR USA.

D. Jiao is with the School of Electrical and Computer Engineering, Purdue University, West Lafayette, IN 47907 USA (e-mail: djiao@purdue.edu).

Color versions of one or more of the figures in this paper are available online at http://ieeexplore.ieee.org.

Digital Object Identifier 10.1109/TAP.2018.2835561

Among existing FDTD subgridding algorithms, the consistency of the field coupling scheme or reciprocity has been widely adopted as a viable means to ensure stability. In other words, if a field unknown A is used to generate a field unknown B, then the field unknown B should also be involved in the generation of the field unknown A. In some algorithms, the coupling coefficient from A to B and vice versa are also enforced to be equal. This certainly limits the accuracy of the interpolation schemes as well as the meshing flexibility in a subgridding scheme.

In this paper, to systematically control the stability of the FDTD subgridding algorithm without sacrificing accuracy, we first reformulate the FDTD algorithm from the original edge-based dual-grid one to a new patch-based single-grid formulation. Using this formulation, we only need to generate one column vector and one row vector for each patch in a single grid, regardless of whether the grid is 2-D or 3-D, it has subgrids or not, and the grid/subgrid is uniform or nonuniform. The product of the column vector and the row vector of each patch is a rank-1 matrix. The system matrix is simply the sum of the rank-1 matrices. Based on this new representation of the FDTD algorithm, the stability of the FDTD-based methods can be readily analyzed for both regular grids and grids having subgrids. In a regular grid, each rank-1 matrix comprising the FDTD system matrix is symmetric positive semidefinite, and hence, the sum of them remains to be positive semidefinite, thus ensuring the stability. In other words, one can always find a time step to make the explicit FDTD time marching stable. However, when subgrids are present, since field unknowns at the interface would have to be interpolated from adjacent unknowns to ensure accuracy, the resultant rank-1 matrix is usually unsymmetrical. When the unsymmetrical matrix has complex-valued or negative eigenvalues, it will make a traditional explicit marching absolutely unstable. However, in general, we cannot rule out these eigenvalues from an unsymmetrical matrix. Even though the unsymmetrical matrix generated from each patch has nonnegative real eigenvalues, we cannot prove that the sum of these unsymmetrical matrices has nonnegative real eigenvalues only. The property of a symmetric matrix does not apply to an unsymmetrical matrix. To overcome this problem, we propose a new time-marching scheme, which preserves the FDTD's advantage in matrix-free time marching while remaining to be stable in the presence of complex and negative eigenvalues. As a result, the proposed method does not require reciprocal operations from one field unknown to the other to guarantee stability. The proposed time-marching scheme is also general, which can be used to make other unsymmetrical FDTD subgridding algorithms stable.

With the stability guaranteed in time, the interpolation schemes can be developed solely to ensure accuracy. We hence develop an accurate interpolation scheme to ensure the accuracy of the resulting subgridding algorithm. This scheme is applicable to arbitrary contrast ratios between the normal gird and the subgrid, as well as supporting nonuniform subgridding. We also show that since there are only a few kinds of rank-1 matrices in the proposed algorithm, the maximum time step permitted for a stable simulation can be analytically analyzed. The proposed subgridding algorithm is then further made unconditionally stable based on our prior work in [15] and [16]. Notice that the focus of this paper is an accurate subgridding algorithm that is unsymmetric yet stable. This is very different from [15] and [16] where a single grid is used, whose focus is an unconditonally stable method. Recently, in [17], we also developed a symmetric positive semidefinite subgridding algorithm. However, this paper is very different as it is *unsymmetric* while still being stable. It provides more flexibility in interpolation for obtaining interface unknowns, since there is no need to preserve a symmetric system. Extensive numerical experiments involving both 2- and 3-D subgrids with various contrast ratios have demonstrated the accuracy, stability, and efficiency of the proposed new subgridding method.

II. Problem Statement

In the original FDTD algorithm, one field unknown is placed in a primary grid at the center point of each edge and also tangential to the edge. The other field unknown is placed in a dual grid in the same way. If there are N_e electric field unknowns and N_h magnetic field unknowns, then there are $N_e + N_h$ equations in the FDTD-based discretization of Maxwell's equations. Essentially, we can view that each equation is written for obtaining one electric or magnetic field unknown, for example, obtaining the time derivative of one electric field unknown from its surrounding magnetic field unknowns and vice versa.

When there is a subgrid present in the discretization, the original FDTD algorithm has to be modified. There are also subgridding techniques that are not purely based on FDTD anymore. However, using the original framework of FDTD on the interface between the normal grid and the subgrid, one would face the following problem. The generation of the primary field unknown would require the dual field unknown at the points that are not coincident with the points where the dual field is generated from the primary field. A natural remedy to this problem is to interpolate the unknown dual field at the desired point from the known dual fields at adjacent points. Such an interpolation scheme is not unique. However, its effect on accuracy and stability is different. A theoretical stability analysis is still lacking in many subgridding algorithms. On the other hand, late-time instability has been observed from many existing techniques. When instability occurs, there is no fundamental way forward to correct the stability problem.

Next, we will first present the proposed theory for making an FDTD subgridding algorithm stable in general subgrid settings. We then proceed to the details of the proposed subgridding method.

III. Proposed Theory

A. Single-Grid Patch-Based FDTD Formulation When Subgrids Are Present

To facilitate the development of a subgridding algorithm, we adopt an alternative formulation of the FDTD. If we term the original FDTD formulation an edge-based dual-grid formulation (as each edge in the primary and dual grid is associated with one field unknown), this alternative formulation is a patch-based single-grid formulation we recently developed in [15] and [16]. In the original formulation, since an edge-based approach is used together with dual grids, when there

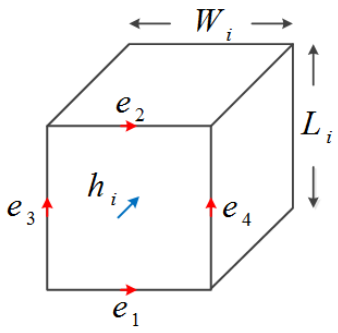

Fig. 1. Illustration of a patch-based discretization of Faraday's law.

are subgrids, there are many scenarios to consider. In contrast, the proposed new formulation is based on patches in a single grid. As a result, the subgridding scenarios to be considered become only a few kinds. Next, we provide a brief review of this new formulation in the context of subgridding.

Consider a general 2-D or 3-D grid. For each patch, based on the FDTD algorithm, we obtain the magnetic field normal to the patch at the patch center, h_i, as follows:

$$\left[-\frac{1}{L_i}, \frac{1}{L_i}, \frac{1}{W_i}, -\frac{1}{W_i}\right]\begin{bmatrix} e_1 \\ e_2 \\ e_3 \\ e_4 \end{bmatrix} = -\mu_i \frac{\partial h_i}{\partial t} \tag{1}$$

where subscript i denotes the patch index and e denotes the tangential electric field at the center point of every edge in the patch, as shown in Fig. 1. L_i and W_i are the two side lengths of patch i, and μ_i is the permeability at the patch center. Equation (1) can be rewritten as

$$[b]_i^T [e]_i = -\mu_i \frac{\partial h_i}{\partial t} \tag{2}$$

where $[e]_i$ denotes the column vector containing all of the electric field unknowns of patch i, and $[b]_i^T$ is a row vector of

$$[b]_i^T = \left[-\frac{1}{L_i}, \frac{1}{L_i}, \frac{1}{W_i}, -\frac{1}{W_i}\right]. \tag{3}$$

If $\{e\}$ is a vector consisting of all N_e electric field unknowns in a grid, (2) can be rewritten as

$$\{b\}_i^T \{e\} = -\mu_i \frac{\partial h_i}{\partial t} \tag{4}$$

in which $\{b\}_i$ is $[b]_i$ in (3) extended to length N_e, such that $\{b\}_i^T\{e\} = [b]_i^T[e]_i$. Obviously, $\{b\}_i$ has only four nonzero entries as follows:

$$\{b\}_i(g(i,k)) = [b]_i(k), \quad k = 1, 2, 3, 4 \tag{5}$$

in which $g(i,k)$ denotes the index of the kth electric field unknown of patch i in the global electric field vector $\{e\}$. Considering all patches present in the mesh, the discretization of Faraday's law can be represented as

$$\mathbf{S}_e\{e\} = -\text{diag}\{\mu\}\frac{\partial\{h\}}{\partial t} \tag{6}$$

where $\{h\}$ contains all of the h unknowns whose number is N_h, diag$\{\mu\}$ is a diagonal matrix of permeability, and $\{b\}_i^T$ is the ith row of $\mathbf{S}_e$.

In a general patch present in a grid with subgridding, the row vector shown in (3) will be different. However, its entries remain to be the weighting coefficients of the electric field unknowns along the contour of a patch for generating the normal magnetic field at the patch center. To be more specific, $[b]_i$ has m entries, where m is the number of electric field unknowns along the contour of patch i. An arbitrary kth entry of $[b]_i$, $[b]_i(k)$, is simply the weighting coefficient of electric field unknown e_k used to generate h_i. Its sign is determined by the right-hand rule. With the right-hand thumb pointing to the direction associated with h_i, if e_k's direction is along the direction encircling the h_i's direction, the sign is positive. Otherwise, the sign is negative.

In the original FDTD formulation, the discretization of Ampere's law is performed on a dual grid, resulting in the following matrix equation:

$$(\mathbf{S}_h)_{N_e \times N_h}\{h\} = \text{diag}\{\epsilon\}\frac{\partial\{e\}}{\partial t} + \{j\} \tag{7}$$

where $\{h\}$ contains all of the h unknowns whose number is N_h, diag$\{\epsilon\}$ is a diagonal matrix of permittivity, and $\{j\}$ denotes a current source vector. Each row of (7) simply denotes a discretized curl operation performed on the magnetic fields producing the time derivative of an electric field.

In the alternative formulation, we rewrite (7) as follows:

$$\{a\}_1 h_1 + \{a\}_2 h_2 + \cdots + \{a\}_{N_h} h_{N_h} = \text{diag}\{\epsilon\}\frac{\partial\{e\}}{\partial t} + \{j\} \tag{8}$$

where the matrix-vector multiplication of $\mathbf{S}_h\{h\}$ in (7) is realized as the sum of weighted columns, instead of the traditional row-based computation which we are more familiar with. Here, $\{a\}_i$ is simply the ith column of $\mathbf{S}_h$, and h_i is the ith entry of vector $\{h\}$, which is nothing but the normal magnetic field at the center of patch i. Based on how Ampere's law is discretized in the FDTD method, it is evident that $\{a\}_i$ has only nonzero entries at the rows whose indexes correspond to the electric field unknowns generated from h_i. In a regular grid, h_i is used to generate four electric field unknowns, which are those along the four sides of patch i. Hence, $\{a\}_i$ has only four nonzero elements, where all the others are zero. Removing the zeros, $\{a\}_i$ simply becomes a vector of length four in each patch as follows:

$$[a]_i = \begin{bmatrix} -\frac{1}{L_i} \\ \frac{1}{L_i} \\ \frac{1}{W_i} \\ -\frac{1}{W_i} \end{bmatrix}. \tag{9}$$

Clearly, it is the same as $[b]_i$ in a uniform grid.

In a general patch present in a grid with subgridding, the column vector $[a]_i$ can become different from that shown in (9). However, its entries remain to be the weighting coefficients of the magnetic field used to generate the electric field unknowns. To be more specific, an arbitrary kth entry of $[a]_i$, $[a]_i(k)$, is simply the weighting coefficient of h_i used to generate e_k.

Though mathematically identical to (7), (8) allows us to discretize Ampere's law in the original grid of $\mathbf{E}$ and

use the same patch-based approach. Basically, to discretize Ampere's law, we also loop over all the patches in the original grid. On each patch, we generate a column vector $\{a\}_i$ $(i = 1, 2, \ldots, N_h)$. Scaling $\{a\}_i$ by h_i and summing it up over all the patches in the original grid, we obtain the discretization of the curl of $\mathbf{H}$, as shown by the left-hand side of (8).

Now, if we take a time derivative of (8) and substitute (4) into it, we obtain

$$\sum_{i=1}^{N_h}\left(\frac{1}{\mu_i}\{a\}_i\{b\}_i^T\right)\{e\} = -\text{diag}\{\epsilon\}\frac{\partial^2\{e\}}{\partial t^2} - \frac{\partial\{j\}}{\partial t} \tag{10}$$

which can be compactly written as

$$\frac{\partial^2\{e\}}{\partial t^2} + \mathbf{C}\{e\} = -\text{diag}\left\{\frac{1}{\epsilon}\right\}\frac{\partial\{j\}}{\partial t} \tag{11}$$

where

$$\mathbf{C} = \text{diag}\left\{\frac{1}{\epsilon}\right\}\sum_{i=1}^{N_h}\frac{1}{\mu_i}\{a\}_i\{b\}_i^T \tag{12}$$

which is clearly the sum of the rank-1 matrix obtained from each patch.

When loss is involved, (11) is augmented by one first-order time derivative as follows:

$$\frac{\partial^2\{e\}}{\partial t^2} + \mathbf{D}_\sigma\frac{\partial\{e\}}{\partial t} + \mathbf{C}\{e\} = -\text{diag}\left\{\frac{1}{\epsilon}\right\}\frac{\partial\{j\}}{\partial t} \tag{13}$$

where $\mathbf{D}_\sigma$ is a diagonal matrix whose entries are σ/ϵ.

In the patch-based formulation, after $[a]_i$ and $[b]_i$ are obtained for each patch, we can use them to perform a leap-frog time marching based on (4) and (8). We can also directly solve (11) or (13) as a second-order differential equation in time.

B. Stability Analysis of FDTD Without and With Subgrids

The stability of the first-order systems (4) and (8) as well as the second-order based (11) is determined by the following eigenvalue problem:

$$\mathbf{C}x = \lambda x. \tag{14}$$

To analyze the stability, we can expand the field solution $\{e\}$ by using the eigenvectors of (14), obtaining

$$\{e\} = \mathbf{V}\{y\} \tag{15}$$

where $\mathbf{V}$ denotes a matrix whose columns are eigenvectors. Substituting (15) into (11) and multiplying both sides of (11) by $\mathbf{V}^T$, we obtain

$$\mathbf{V}^T\mathbf{V}\frac{\partial^2\{y\}}{\partial t^2} + \mathbf{V}^T\mathbf{C}\mathbf{V}\{y\} = 0 \tag{16}$$

where source is removed as it is irrelevant to the stability analysis. Since $\mathbf{V}^T\mathbf{C}\mathbf{V} = \mathbf{V}^T\mathbf{V}\Lambda$, where Λ is the diagonal matrix of eigenvalues λ_i, (16) becomes

$$\frac{\partial^2 y_i}{\partial t^2} + \lambda_i y_i = 0, \quad (i = 1, 2, \ldots, N_e). \tag{17}$$

Performing a z-transform of the above, if all the eigenvalues λ_i are nonnegative real, a time marching based on central difference scheme would be stable as long as

$$\Delta t < \frac{2}{\sqrt{\lambda_{\max}}} \tag{18}$$

where $\lambda_{\max}$ is the largest eigenvalue. In this case, (11) can be marched on in time explicitly as

$$\{e\}^{n+1} = (2-\Delta t^2\mathbf{C})\{e\}^n - \{e\}^{n-1} - \Delta t^2\text{diag}\left\{\frac{1}{\epsilon}\right\}\left(\frac{\partial\{j\}}{\partial t}\right)^n. \tag{19}$$

For a lossy system, as shown in [18], the time step is also governed by (18), where $\lambda_{\max}$ is the maximum eigenvalue of $\mathbf{C}$.

However, when the eigenvalues of $\mathbf{C}$ are complex-valued or negative, no time step can make (17) stable [18]. In an FDTD subgridding scheme, since interpolations are used to obtain the unknown fields at the subgrid interfaces, the resulting rank-1 matrix of each patch is not symmetric. The same is true for the global system matrix assembled from each patch's contribution. An unsymmetric matrix can have complex-valued eigenvalues or even negative ones. In many cases, one can prove the eigenvalues of Maxwell's system to be nonnegative if they are real. However, in general, the complex eigenvalues cannot be ruled out. This can also be numerically verified. When this happens, an FDTD subgridding algorithm is absolutely unstable.

C. How to Guarantee Stability When the System Matrix Is Unsymmetric?

The aforementioned stability problem for an unsymmetric matrix can be resolved by first employing a backward-difference scheme to discretize (11) as follows:

$$(\mathbf{I} + \Delta t^2\mathbf{C})\{e\}^{n+1} = 2\{e\}^n - \{e\}^{n-1} \tag{20}$$

$$- \Delta t^2\text{diag}\left\{\frac{1}{\epsilon}\right\}\left(\frac{\partial\{j\}}{\partial t}\right)^{n+1}. \tag{21}$$

Since a backward-difference scheme is unconditionally stable, we are allowed to use an arbitrarily large time step. However, by doing so, we have to solve a system matrix of $(\mathbf{I} + \Delta t^2\mathbf{C})$. To retain the matrix-free merit of the FDTD, we can choose the following time step to perform the backward time marching:

$$\Delta t < \frac{1}{\sqrt{|\lambda_{\max}|}}. \tag{22}$$

With the above, $\rho(\Delta t^2\mathbf{C}) = |\Delta t^2\lambda_{\max}| < 1$ is satisfied, where $\rho(\cdot)$ denotes the spectral radius of $(\cdot)$. Hence, the inverse of $\mathbf{I} + \Delta t^2\mathbf{C}$ becomes explicit, which can be evaluated as

$$(\mathbf{I} + \Delta t^2\mathbf{C})^{-1} = \mathbf{I} - \Delta t^2\mathbf{C} + (\Delta t^2\mathbf{C})^2 - \cdots. \tag{23}$$

The above series can be truncated at the kth term without sacrificing accuracy, where k is usually less than 10 as (22) is satisfied. Since (23) does not involve any matrix inversion, we can still obtain the solution in (20) explicitly as follows:

$$\{e\}^{n+1} = (\mathbf{I} - \Delta t^2\mathbf{C} + \cdots + (-1)^k(\Delta t^2\mathbf{C})^k)\{f\} \tag{24}$$

where $\{f\}$ denotes the terms moved to the right-hand side.

Therefore, no matter whether the system matrix $\mathbf{C}$ is symmetric or not, we can find the solution explicitly via

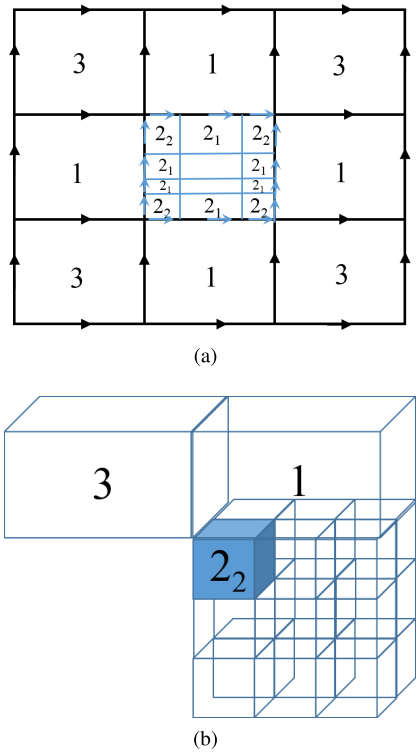

Fig. 2. Illustration of a grid with subgrids. (a) 2-D. (b) 3-D.

either (19) or (24) without incurring any instability. More importantly, the choice of the time step shown in (22) also agrees with the choice of the time step of the traditional explicit time marching. Hence, we do not sacrifice in the size of time step while making the inverse of the backward-difference-based system matrix explicit.

IV. Proposed Subgridding Algorithm With Guaranteed Stability and Accuracy

In an FDTD grid with subgrids, the patches can be categorized into two big classes. One has its regular $[a]$ and $[b]$ vectors. The other class of patches has modified $[a]$ and $[b]$ vectors, because the fields along the subgrid edges have to be obtained through interpolations across patches to ensure accuracy. Based on the stability analysis in Section III-B, it is not necessary to have the two curl operators to be reciprocal to guarantee stability, and thus, the interpolation scheme can be made very flexible. Since the field solution in the FDTD algorithm is known along three orthogonal directions in an orthogonal grid, the interpolation can be carried out in three directions to achieve good accuracy. In this section, we develop a novel FDTD subgridding algorithm with a guaranteed accuracy. This algorithm supports an arbitrary contrast ratio of the regular grid size to the subgrid size. It also allows for nonuniform grids in both regular and subgrid regions.

Considering a regular grid involving subgrids as shown in Fig. 2(a) and (b), we place all of the electric field unknowns along the edges of the grid and at the center of each edge. Thus, our $\{e\}$ is composed of tangential electric field along each edge in the regular grid (regular edge), in the subgrid (subgrid internal edge), and on the interface between the regular grid and the subgrid (subgrid interface edge), as shown in Fig. 2(a). The magnetic field unknown is placed at the center of each patch, along the normal direction of the patch. Thus, $\{h\}$ consists of the magnetic fields normal to each patch at the patch center. It is also worth mentioning that although both positive and negative directions can be chosen as the reference direction of the electric field unknown along each edge, we choose the conventional positive x-, y-, and z-directions. The same is true for the reference direction of the normal magnetic field at the patch center.

A. Building Column Vector $[a]$ and Row Vector $[b]^T$ for Each Patch With Guaranteed Accuracy

A grid can involve many patches. However, we find that regardless of a 2-D or 3-D grid, the patches can be categorized into three irregular types based on their corresponding $[a]$ and $[b]$ vectors. This is attributed to the proposed patch-based formulation, which makes the resultant subgridding algorithm suitable for both 2-D and 3-D grids with almost no change. Next, we elaborate the construction of $[a]$ and $[b]$ vectors for each type of the irregular patches.

1) Irregular Patch Type 1: This patch is a coarse patch in the regular-grid region, but having at least one side shared with the subgrid region, as shown by the patches marked as 1 in Fig. 2(a) and (b). For convenience of explanation, we consider one side with subgridding. Along this side, there are more than one edges due to subgridding. Let the number of edges on this side be n, and the length of the jth edge be l_j. The l_j can be the same for all edges. It can also be different in different edges, as shown in Fig. 2(a).

To generate the magnetic field at the coarse patch center, we need to use the tangential electric field at the center of each side. For the side having subgrids, the electric field unknowns are placed at the center of each subgrid edge. Hence, the electric field at the center of the side needs to be obtained from the subgrid electric fields. This can be accurately done as follows:

$$e_c = \sum_{j=1}^{n} \frac{l_j}{L_i} e_j \tag{25}$$

in which L_i is the entire length of the side, where subscript i denotes the patch index. The resulting row vector $[b]_i^T$ for this patch can be written as

$$[b]_i^T = \left[-\frac{1}{L_i}, \frac{1}{L_i}, \frac{1}{W_i}, -\frac{1}{W_i} v^T \right] \tag{26}$$

where

$$v^T = \left[\frac{l_1}{L_i}, \frac{l_2}{L_i}, \ldots, \frac{l_n}{L_i} \right]. \tag{27}$$

Hence, $[b]_i^T$ is no longer of length 4, but of length $3+n$. The accuracy of the resulting (2) is of second order. This is because if we perform a line integral of the electric field along the contour of the patch using the electric field unknowns located on the contour, and equate it to $-\mu(\partial h_i/\partial t)$ at the patch center multiplied by the patch area, we will obtain (26).

The above $[b]_i^T$ is written for the case when the fourth electric field in a patch is associated with the subgrids. If it is another electric field, say the jth electric field, the v^T is multiplied to the jth entry of the original $[b]_i^T$, and the

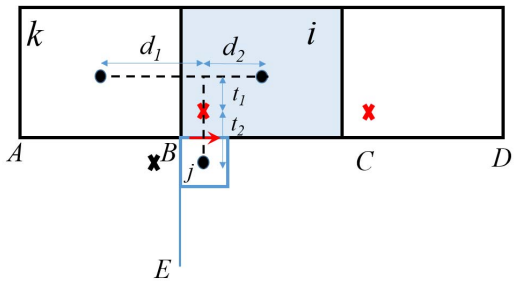

Fig. 3. Illustration of the interpolation scheme.

denominator of (27) should be changed to the length of the side having subgrids. If there are multiple sides shared with the subgrid region, then v^T will be attached to each entry associated with the subgridding side.

To construct column vector $[a]_i$ for this patch, we need to find out how the magnetic field at this patch is used to generate electric field unknowns. Within this patch, the electric field unknown along the regular edge is obtained from the magnetic field at the center of this patch and the other one at the center of the adjacent patch sharing the regular edge. Hence, the corresponding entry in $[a]_i$ is the same as that in a regular discretization, which is $\pm(1/L_i)$, $\pm(1/W_i)$, or another one if a nonuniform grid is used. However, to ensure accuracy, the electric field along the subgrid interface edge cannot be obtained in the same way. Taking one subgrid interface edge highlighted by a red arrow in Fig. 3 as an example, to obtain the electric field accurately at the edge center, we need to know the magnetic field at the point marked by $\times$ above the red arrow. Since the magnetic fields are only known at the center of every patch, the magnetic field at this point has to be interpolated. Here, we perform a linear interpolation using the magnetic fields at adjacent patches, since it can provide a second-order accuracy.

To explain this interpolation scheme, let the coarse patch being considered be patch i. The subgrid interface edge must be shared by patch i and a fine patch in the subgrid. Let this fine patch be patch j, as shown in Fig. 3. Let the magnetic fields at the center points of the two patches be, respectively, h_i^c and h_j^f, where we use the superscript to indicate whether the patch is coarse or fine. To interpolate the magnetic field at the marked point accurately, we also find another coarse patch k. This patch and patch i share a regular edge in common, and this regular edge is perpendicular to the subgrid edge and closer to the subgrid edge in between the two regular edges of patch i. We denote the magnetic field at the center of this patch by h_k^c. The magnetic field at the marked point can then be accurately interpolated as

$$h_\times = \frac{t_2}{t}\left(\frac{d_2}{d}h_k^c + \frac{d_1}{d}h_i^c\right) + \frac{t_1}{t}h_j^f \tag{28}$$

where t_1, t_2, d_1, and d_2 are distances labeled in Fig. 3, and $t = t_1 + t_2$ and $d = d_1 + d_2$. These distances can be readily found from the coordinates of the three patch centers. Obviously, a linear interpolation along all directions is used to obtain the magnetic field at the marked point. With $h_\times$, the electric field at the subgrid interface edge can be accurately obtained from the magnetic field at the fine patch center and that at the marked point as follows:

$$\epsilon\frac{\partial e_j}{\partial t} = \frac{h_j^f - h_\times}{W_j^f}. \tag{29}$$

Substituting (28) into (29), obviously, the coefficient in front of h_i for generating e_j is $-(1/W_j^f)c_j$, where $c_j = (t_2/t)(d_1/d)$ and the distance parameters are those corresponding to the jth subgrid edge.

The aforementioned interpolation results in the following $[a]_i$ vector:

$$[a]_i = \begin{bmatrix} -\dfrac{1}{L_i} \\ \dfrac{1}{L_i} \\ \dfrac{1}{W_i} \\ -u \end{bmatrix} \tag{30}$$

in which u is a vector of

$$u = \begin{bmatrix} \dfrac{c_1}{W_1^f} \\ \dfrac{c_2}{W_2^f} \\ \vdots \\ \dfrac{c_k}{W_k^f} \end{bmatrix} \tag{31}$$

where W_j^f is the width of the fine patch whose electric field is generated from h_i and c_j $(j = 1, 2, \ldots k)$ are positive coefficients between 0 and 1. Here, k can be greater than n, because the magnetic field at patch i may also be used to obtain electric fields not belonging to patch i. To be specific, on the patch i being considered, we can generate n such c-coefficients, where n is the number of subgrid edges on the side having subgrids. As shown in Fig. 3, this is the number of subgrid edges on side BC. The rest of $k-n$ entries in u are due to other electric field unknowns generated from h_i. In the following, we will give a complete count of these electric field unknowns.

In a 2-D setting, if along the adjacent sides of BC, namely, right half of AB and left half of CD, there are subgrids, then the electric fields on these subgrid edges will have to be generated from h_i. This is because h_i will be used to interpolate the missing magnetic field required to generate the electric fields on those edges, as highlighted by a red mark adjacent to CD. The same linear interpolation as shown in (28) can be used, from which the corresponding c_j coefficient can be identified. In a 3-D setting, the three sides of AB, BC, and CD become six patches perpendicular to patch i and centering patch i, with three on one side of patch i and the other three on the other side of patch i. All the subgrid edges on the six patches along the direction of BC will be related to h_i. The electric field unknowns on these edges will be interpolated in the same way, as shown in Fig. 3. If coarse patches i and k for the subgrid edge do not exist (this can happen for a subgrid edge falling onto the face of a subgrid region), the adjacent coarse patches parallel to the imaginary patch i and k can be used to interpolate magnetic fields at the center points of imaginary patch i and k and

subsequently used in (28). The resultant c_j coefficients in front of h_i remain to be between 0 and 1. Regardless of 2-D and 3-D, since the electric field unknowns to be generated from h_i on patch i are all orientated in the same direction, the sign of their corresponding entries in $[a]_i$ is the same. If there are multiple sides shared with the subgrid region in patch i, similarly, vector u will appear at the corresponding entry and follow the original sign of the entry.

2) Irregular Patch Type 2: For this type, the patch is a fine patch in the subgrid but with at least one side falling onto the subgrid interface with the regular grid. This type of patches is illustrated by patches marked by 2_2 and 2_1 in Fig. 2(a) and (b), where subscript denotes the number of edges on the interface.

In such a patch, $[b]_i^T$ remains the same as that in a regular grid, but the length and width used are the fine-patch counterparts. Thus, we have

$$[b]_i^T = \left[-\frac{1}{L_i}, \frac{1}{L_i}, \frac{1}{W_i}, -\frac{1}{W_i}\right]. \tag{32}$$

However, $[a]_i$ is different. Again, to determine $[a]_i$, we need to find out how the magnetic field at this patch is used to generate electric field unknowns. Within the patch, among the four electric field unknowns, two are not located on the interface and thereby shared by two fine patches. They are generated from h_i in the same way as the regular ones. For the two residing on the interface, each of them requires one magnetic field that is outside the subgrid and unknown, as shown by the marks in Fig. 3. Again, such a magnetic field is interpolated from the magnetic fields at the three patch centers in the same way, as shown in (28). Hence, the resultant $[a]_i$ vector is

$$[a]_i = \begin{bmatrix} -\dfrac{1}{L_i} \\ \dfrac{1}{L_i}(1-c_2) \\ \dfrac{1}{W_i}(1-c_3) \\ -\dfrac{1}{W_i} \end{bmatrix} \tag{33}$$

where c_2 and c_3 are positive coefficients between 0 and 1. Based on (28), they have the form of $c_j = (t_1/t)$ in which t_1 and t are distance parameters associated with the subgrid edge residing on the interface. If only one edge of the fine patch falls onto the interface between a regular grid and a subgrid, only one c coefficient is present. If edges 2 and 3 are not on the interface but other edges, (33) can be simply permuted.

In addition, the magnetic field at this subgrid patch may also be used to obtain electric fields elsewhere not belonging to this patch. This can happen when the coarse patch has two sides or more having subgrids. In this case, (33) will have more than four entries, whose value can be readily determined from the interpolation of the pertinent electric field unknown from this patch's magnetic field. However, regardless of the number of other electric field unknowns generated from this patch's magnetic field, $[b]_i^T$ is zero corresponding to these other electric field unknowns.

3) Irregular Patch Type 3: This type of patches is a coarse patch without any subgrid edges, i.e., it consists of the regular edges only, as marked by patch 3 in Fig. 2(a) and (b). However, the magnetic field at this patch is used to generate electric fields elsewhere, and hence, the resultant $[a]_i$ vector is different from the regular one. This type of patches is those patches that are connected with the subgrids through vertices in both the 2- and 3-D grids.

In this type of patches, $[b]_i^T$ remains the same as

$$[b]_i^T = \left[-\frac{1}{L_i}, \frac{1}{L_i}, \frac{1}{W_i}, -\frac{1}{W_i}\right] \tag{34}$$

since four electric fields along the patch contour produce the magnetic field at the patch center.

The $[a]_i$ vector, however, takes the following irregular form:

$$[a]_i = \begin{bmatrix} -\dfrac{1}{L_i} \\ \dfrac{1}{L_i} \\ \dfrac{1}{W_i} \\ -\dfrac{1}{W_i} \\ \dfrac{c_1}{L_1^f} \\ \vdots \\ \dfrac{c_k}{L_k^f} \end{bmatrix} \tag{35}$$

where $c_j (j = 1, 2, \ldots k)$ are interpolation coefficients whose absolute value is between 0 and 1, but can be either positive or negative, k is the number of electric fields that are generated from the magnetic field at this patch center, and L_j^f are the length parameter of the fine patch that has electric field j.

We can also have a complete count of the electric field unknowns generated from type-3 h_i. Take patch k shown in Fig. 3 as an example, and it belongs to type 3. All the electric field unknowns along the left half of BC and upper half of BE that have subgrids will have one entry in $[a]_i$ of patch k. In 3-D settings, the side of BC becomes two patches (of a coarse patch size) perpendicular to patch k and centering patch k. All electric field unknowns along the subgrid edges on the two patches and parallel with BC will be generated from h_k. Similarly, the side of BE also becomes two patches perpendicular to patch k and also centering patch k. All electric field unknowns along the subgrid edges on the two patches and parallel with BE will be generated from h_k. The above can be extended to the rest of three vertices of patch k, if through those vertices, patch k is also attached to subgrids.

B. Estimation of Maximum Time Step

Due to the interpolation scheme, the time step estimated from the Courant–Friedrichs–Lewy condition can be inaccurate for a mesh involving subgrids. Although the maximum time step can be calculated from the largest eigenvalue of the system matrix, calculating eigenvalues of the global matrix can be computationally expensive especially when the matrix size is large, and thus, we should find an efficient way to estimate the time step accurately.

One way is to use matrix norm. Since the spectral radius of a matrix is bounded from the above by its matrix norm, we can estimate the norm of the global system matrix $\mathbf{C}$ by analyzing each rank-1 matrix, thus providing an upper bound of the time

step used for time marching. Since the system matrix $\mathbf{C}$ can be represented as $\text{diag}\{1/\epsilon\}\mathbf{S}_h\text{diag}\{1/\mu\}\mathbf{S}_e$, we have

$$\rho(\mathbf{C}) \le \|\mathbf{C}\| \le \|\text{diag}\{1/\epsilon\}\mathbf{S}_h\|\|\text{diag}\{1/\mu\}\mathbf{S}_e\| \tag{36}$$

which is true independent of the type of the norm used. For example, if 1-norm is used, the above can be written as

$$\rho(\mathbf{C}) \le \|\text{diag}\{1/\epsilon\}\mathbf{S}_h\|_1\|\text{diag}\{1/\mu\}\mathbf{S}_e\|_1 \tag{37}$$

which is further bounded by

$$\rho(\mathbf{C}) \le \|\text{diag}\{1/\epsilon\}\mathbf{S}_h\|_1\|\text{diag}\{1/\mu\}\mathbf{S}_e\|_\infty \tag{38}$$

because the infinity norm (maximum absolute row sum) of $\mathbf{S}_e$ is no less than its 1-norm (maximum absolute column sum) based on the structure of $\mathbf{S}_e$. Since each column of $\mathbf{S}_h$ is an $\{a\}_i$ vector and each row of $\mathbf{S}_e$ is a $\{b\}_i^T$ vector, the above bound can be quickly evaluated from $\{a\}_i$ and $\{b\}_i^T$ of the rank-1 matrix of each patch. To be specific, the patch whose column vector $\{a\}_i$ has the largest norm determines $\|\text{diag}\{1/\epsilon\}\mathbf{S}_h\|$, and the patch whose row vector $\{b\}_i^T$ has the largest norm determines $\|\text{diag}\{1/\mu\}\mathbf{S}_e\|_1$. Hence,

$$\rho(\mathbf{C}) \le \frac{1}{\epsilon_{\min}\mu_{\min}}(\max_i \|\{a\}_i\|_1)(\max_i \|\{b\}_i\|_1) \tag{39}$$

where subscript $_{\min}$ denotes the smallest entry.

The aforementioned method provides an upper bound that may overestimate the actual spectral radius of $\mathbf{C}$. Next, we propose another method to provide a more accurate bound of the time step in a subgridding scheme.

We first rewrite (11) as

$$\frac{\partial^2\{\tilde{e}_i\}}{\partial t^2} + \mathbf{C}_i\{e\} = -\text{diag}\left\{\frac{1}{\epsilon}\right\}\frac{\partial\{j\}_i}{\partial t}, \quad (i = 1, \ldots, N_h) \tag{40}$$

where

$$\{e\} = \{\tilde{e}_1\} + \{\tilde{e}_2\} + \cdots + \{\tilde{e}_{N_h}\} \tag{41}$$

$\mathbf{C}_i$ is the rank-1 matrix of patch i, and

$$\mathbf{C} = \mathbf{C}_1 + \mathbf{C}_2 + \cdots + \mathbf{C}_{N_h}. \tag{42}$$

Obviously, adding the N_h equations in (40), we obtain the original equation (11). The N_h sets of equations in (40) can be compactly written as

$$\frac{\partial^2\{\tilde{e}\}}{\partial t^2} + \tilde{\mathbf{C}}\{\tilde{e}\} = -\text{diag}\left\{\frac{1}{\epsilon}\right\}\frac{\partial\{\tilde{j}\}}{\partial t} \tag{43}$$

where $\{\tilde{e}\} = \{\tilde{e}_1, \tilde{e}_2, \ldots, \tilde{e}_{N_h}\}^T$, and

$$\begin{aligned}\tilde{\mathbf{C}} &= \begin{bmatrix} \mathbf{C}_1 & 0 & 0 & \cdots & 0 \\ 0 & \mathbf{C}_2 & 0 & \cdots & 0 \\ \vdots & & & & \\ 0 & 0 & 0 & \cdots & \mathbf{C}_{N_h} \end{bmatrix}\begin{bmatrix} \mathbf{I} & \mathbf{I} & \mathbf{I} & \cdots & \mathbf{I} \\ \mathbf{I} & \mathbf{I} & \mathbf{I} & \cdots & \mathbf{I} \\ \vdots & & & & \\ \mathbf{I} & \mathbf{I} & \mathbf{I} & \cdots & \mathbf{I} \end{bmatrix} \\ &= \mathbf{C}_d\mathbf{I}_f\end{aligned} \tag{44}$$

which is a block diagonal matrix $\mathbf{C}_d$ made of each patch's rank-1 matrix, multiplied by $\mathbf{I}_f$ whose block entry is $\mathbf{I}$. $\mathbf{I}_f$ is symmetric, whose 2-norm is also its spectral radius. This spectral radius can be readily found as 1, since its nonzero eigenvalue can be analytically found to be 1. As for the block diagonal matrix $\mathbf{C}_d$, its 2-norm is also its spectral radius, because it is symmetric. Hence, the eigenvalue of a single patch's matrix, whose value is the largest among all $\mathbf{C}_i$ values, determines the spectral radius of $\tilde{\mathbf{C}}$ as follows:

$$\rho(\tilde{\mathbf{C}}) \le \|\mathbf{C}_d\|_2\|\mathbf{I}_f\|_2 = \rho(\mathbf{C}_d) = \max_i(\rho(\mathbf{C}_i)). \tag{45}$$

$\rho(\mathbf{C}_i)$ is nothing but

$$\rho(\mathbf{C}_i) = \{b\}_i^T\{a\}_i. \tag{46}$$

This is because each $\mathbf{C}_i$ is a rank-1 matrix whose form is $\{a\}_i\{b\}_i^T$. For such a matrix, it has only one nonzero eigenvalue, which can also be analytically found as $\{b\}_i^T\{a\}_i$ [16].

Since (11) is equivalent to (43), the time step for an explicit yet stable simulation is bounded by

$$\Delta t \le \frac{2}{\sqrt{\max_i(\rho(\mathbf{C}_i))}} = \frac{2}{\sqrt{\max_i\left(\{b\}_i^T\{a\}_i\right)}}. \tag{47}$$

As a result of the proposed method, the computational cost is negligible to determine the choice of the time step. Since there are only a few types of patches, thus $\mathbf{C}_i$, the maximum of their spectral radius can also be readily identified. Next, we provide a quantitative analysis for each type of patch.

1) Regular Patch (in a Uniform or Nonuniform Grid): In both 2- and 3-D settings, the patches that are not adjacent to the interface between a regular grid and a subgrid are considered as regular patches. Their corresponding rank-1 matrices are

$$\mathbf{C}_0 = \begin{bmatrix} -\dfrac{1}{L_i} \\ \dfrac{1}{L_i} \\ \dfrac{1}{W_i} \\ -\dfrac{1}{W_i} \end{bmatrix}\left[-\frac{1}{L_i}, \frac{1}{L_i}, \frac{1}{W_i}, -\frac{1}{W_i}\right] \tag{48}$$

where we omit the permittivity and permeability for convenience.

Based on [16], the eigenvalue of a rank-1 matrix of $\{a\}\{b\}^T$ is $\{b\}^T\{a\}$, and hence, we have

$$\rho(\mathbf{C}_0) = \frac{2}{L_i^2} + \frac{2}{W_i^2}. \tag{49}$$

If $L_i = W_i$, the above is simply $4/{L_i}^2$.

In a nonuniform grid, the average width of the two patches sharing the electric field edge is, in general, used for achieving a better accuracy. In this case, $\mathbf{C}_0$ becomes

$$\mathbf{C}_0 = \begin{bmatrix} -\dfrac{1}{L1_i} \\ \dfrac{1}{L2_i} \\ \dfrac{1}{W1_i} \\ -\dfrac{1}{W2_i} \end{bmatrix}\left[-\frac{1}{L_i}, \frac{1}{L_i}, \frac{1}{W_i}, -\frac{1}{W_i}\right] \tag{50}$$

where the length parameters $L1, L2, W1$, and $W2$ are averaged between two patches sharing the electric field edge. The spectral radius of $\mathbf{C}_0$ should also be calculated accordingly.

2) Irregular Patch Type 1: For every patch of this type, the corresponding rank-1 matrix has the following form:

$$\mathbf{C}_1 = \begin{bmatrix} -\frac{1}{L_i} \\ \frac{1}{L_i} \\ \frac{1}{W_i} \\ -u \end{bmatrix} \left[-\tfrac{1}{L_i}, \tfrac{1}{L_i}, \tfrac{1}{W_i}, -\tfrac{1}{W_i}\tilde{v}^T \right] \tag{51}$$

in which $\tilde{v}$ is the v shown in (27) extended to length k by appending zeros at the end if $k > n$. For this rank-1 matrix, its eigenvalue is

$$\rho(\mathbf{C}_1) = \frac{2}{L_i^2} + \frac{1}{W_i^2} + \frac{1}{W_i}\tilde{v}^T u. \tag{52}$$

3) Irregular Patch Type 2: For this type of patches, the corresponding rank-1 matrix has the following form:

$$\mathbf{C}_2 = \begin{bmatrix} -\frac{1}{L_i} \\ \frac{1}{L_i}(1-c_2) \\ \frac{1}{W_i}(1-c_3) \\ -\frac{1}{W_i} \end{bmatrix} \left[-\frac{1}{L_i}, \frac{1}{L_i}, \frac{1}{W_i}, -\frac{1}{W_i} \right] \tag{53}$$

where c_2 and c_3 are nonzero or one of them is zero. When they are nonzero, they are positive coefficients between 0 and 1. More nonzero entries can also appear in the column vector $\{a\}$ for this patch depending on the subgrid configuration. However, since the row vector $\{b\}$ has only four nonzero entries, the eigenvalue of this matrix is

$$\rho(\mathbf{C}_2) = \frac{2-c_2}{L_i^2} + \frac{2-c_3}{W_i^2}. \tag{54}$$

4) Irregular Patch Type 3: For every patch of this kind, the corresponding rank-1 matrix has the following form:

$$\mathbf{C}_3 = \begin{bmatrix} -\frac{1}{L_i} \\ \frac{1}{L_i} \\ \frac{1}{W_i} \\ -\frac{1}{W_i} \\ \frac{c_1}{L_1^f} \\ \vdots \\ \frac{c_k}{L_k^f} \end{bmatrix} \left[-\frac{1}{L_i}, \frac{1}{L_i}, \frac{1}{W_i}, -\frac{1}{W_i}, zeros(1,k) \right] \tag{55}$$

where c_j $(j = 1, \ldots, k)$ are interpolation coefficients that can be either positive or negative, and k zeros are appended at the end of the row vector. The spectral radius of $\mathbf{C}_3$ can be readily calculated as

$$\rho(\mathbf{C}_3) = \frac{2}{L_i^2} + \frac{2}{W_i^2}. \tag{56}$$

From the aforementioned analysis, it can be seen clearly that for an explicit time marching, the time step of the proposed subgridding scheme is determined by the fine patch residing in the fine grid, since such a patch has the largest eigenvalue.

V. Explicit FDTD Subgridding Algorithm With Unconditional Stability

In the existing FDTD subgridding algorithms, temporal subgridding schemes have also been developed to take advantage of the large time step size permitted by the coarse grid and localize the use of small time step in the subgrid region. In this paper, we will leverage our prior work in [15] to make the entire scheme unconditionally stable while still being explicit. In other words, one can use a large time step size for both regular and subgrid regions.

In a subgridding mesh, if the coarse grid size is chosen based on accuracy requirements, the time step required by stability can be estimated as the time step required by accuracy divided by contrast ratio CR from the analysis of Section IV. When CR is large, the time step required by stability is much smaller than that required by accuracy. To tackle this problem, one can separate the unknowns in the coarse grid from those in subgrids and solve them in an explicit-implicit fashion. One can also resort to temporal subgridding schemes. Here, we provide an approach based on [15], where the source of instability is found from the fine region and deducted from the system matrix. As a result, an explicit FDTD subgridding algorithm can also be made unconditionally stable. This permits the use of a large time step size, solely determined by accuracy regardless of space step, in both regular and subgrid regions.

Given any desired time step Δt, we first categorize all the cells in the grid into two groups. One group $\mathbb{G}_c$ has regular cell sizes and permits the use of the desired time step, while the other group $\mathbb{G}_f$ includes all the fine cells in the subgrids and their adjacent cells that require a smaller time step for a stable simulation. Accordingly, $\mathbf{C}$ can be split into the following two components:

$$\mathbf{C} = \mathbf{C}_f + \mathbf{C}_c \tag{57}$$

where $\mathbf{C}_f$ is assembled from $\mathbb{G}_f$ and $\mathbf{C}_c$ is from $\mathbb{G}_c$. Based on (12), $\mathbf{C}_f$ can be obtained by summing up the rank-1 matrix over all the patches in $\mathbb{G}_f$ and hence being

$$\mathbf{C}_f = \text{diag}\left\{\frac{1}{\epsilon}\right\} \sum_{i=1,\ i\in\mathbb{G}_f}^{p} \frac{1}{\mu_i}\{a\}_i\{b\}_i^T \tag{58}$$

in which p is the number of patches in the group $\mathbb{G}_f$.

Let the $\mathbf{E}$ and $\mathbf{H}$ unknown number in $\mathbb{G}_f$ be q and p, respectively. If we eliminate the zero rows of $\{a\}_i$ and zero columns of $\{b\}_i^T$, (58) becomes a small $q \times q$ matrix, which can be written as

$$\mathbf{C}_f^{(f)}{}_{q\times q} = \mathbf{A}_{q\times p}\mathbf{B}_{p\times q}^T \tag{59}$$

where $\mathbf{A}$ stores all the p column vectors and $\mathbf{B}^T$ consists of all the row vectors. We then find the largest l eigenvalues λ_i and their corresponding eigenvectors $\mathbf{F}_{hi}^{(f)}$ of $\mathbf{C}_f$ by using the Arnoldi method. The complexity of doing so is only $O(l^2 q)$. To check whether $\mathbf{F}_{hi}^{(f)}$ are accurate approximations of the

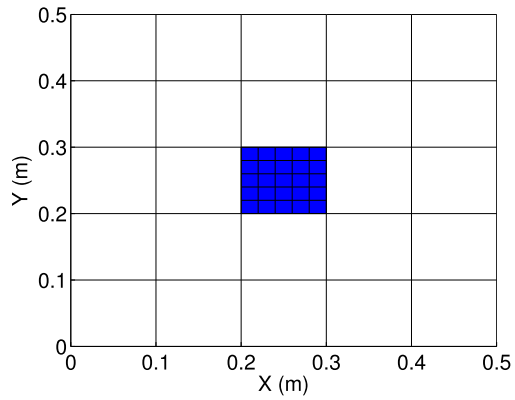

(a)

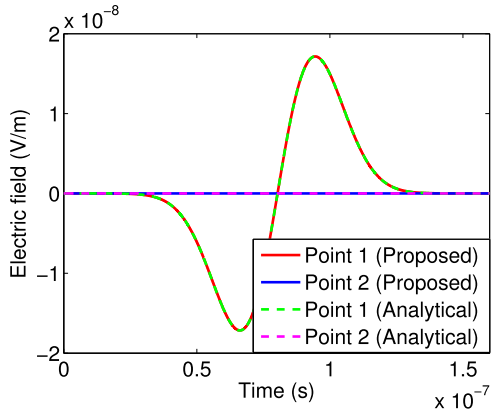

(b)

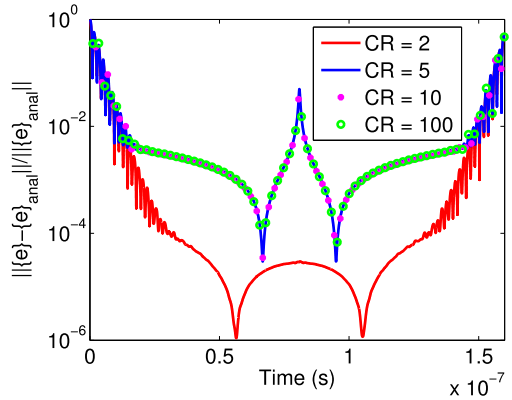

(c)

Fig. 4. Simulation of a 2-D wave propagation problem. (a) Mesh details. (b) Simulated electric field at two observation points in comparison with reference analytical solutions. (c) Entire solution error versus time for different contrast ratios.

original eigenvectors of $\mathbf{C}$, we extend $\mathbf{F}_{hi}^{(f)}$ to $\mathbf{F}_{hi}$ of length N_e based on global unknown ordering. We then perform the following accuracy check:

$$\frac{\|\mathbf{C}\mathbf{F}_{hi} - \lambda_i \mathbf{F}_{hi}\|}{\|\mathbf{C}\mathbf{F}_{hi}\|} < \epsilon. \tag{60}$$

Those $\mathbf{F}_{hi}$ values satisfying the above accuracy requirement are then identified as the unstable modes. They are first orthogonalized to be $\mathbf{V}_h$ and then deducted from the system

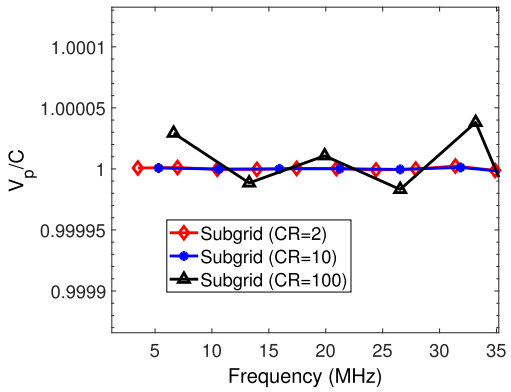

Fig. 5. Ratio of numerical phase velocity to the speed of light as a function of frequency for different grid ratios.

matrix as follows:

$$\mathbf{C}_l = \mathbf{C} - \mathbf{V}_h \mathbf{V}_h^H \mathbf{C}. \tag{61}$$

The above allows for a much larger time step than $\mathbf{C}$. We then perform explicit marching on the updated system matrix as

$$\{e\}^{n+1} = 2\{e\}^n - \{e\}^{n-1} - \Delta t^2 \mathbf{C}_l \{e\}^n + \Delta t^2 \{f\}^n \tag{62}$$

followed by the following treatment to ensure that the resultant $\{e\}$ has no component in the $\mathbf{V}_h$ space:

$$\{e\}^{n+1} = \{e\}^{n+1} - \mathbf{V}_h \mathbf{V}_h^H \{e\}^{n+1}. \tag{63}$$

Since the contribution of $\mathbf{V}_h$ is removed from $\mathbf{C}$, the time marching of (62) is stable for the desired large time step. When the time step is chosen based on accuracy, the removed $\mathbf{V}_h$ modes are not required for accuracy either [15], [18], [20], hence ensuring accuracy.

VI. Numerical Results

In this section, we simulate a variety of 2- and 3-D examples involving different subgrids to demonstrate the validity and efficiency of the proposed method. The time step is determined by the method described in IV-B, specifically (47). If the unconditionally stable method is used, then the time step is determined by the sampling accuracy for the given input.

A. 2-D Wave Propagation

We first simulate a wave propagation problem in a 2-D rectangular region. The grid is shown in Fig. 4(a). Along both the x- and y-axes, the coarse grid size is $L_c = 0.1$ m. To examine the validity of the proposed FDTD subgridding method, the blue region is subdivided into fine grids where the fine grid size is controlled by contrast ratio $CR = \Delta L_c / \Delta L_f$. Fig. 4(a) shows the mesh details when $CR = 5$. The incident electric field is $\mathbf{E}^{\text{inc}} = \hat{y} 2(t - t_0 - x/c) e^{-(t-t_0-x/c)^2/\tau^2}$ with $c = 3\times10^8$ m/s, $\tau = 2\times10^{-8}$ s, and $t_0 = 4\tau$. All the boundary unknowns are terminated by exact absorbing boundary condition. To check the accuracy of the proposed FDTD subgridding method when $CR = 2$, we first sample the electric field at two observation points located at (0.1, 0.05) m and (0.275, 0.3) m and plot it in Fig. 4(b). Point 1 is inside the coarse mesh, while point 2 is on the boundary of the subgridding region. The reference result we use here is the analytical solution.

TABLE I
SIMULATION PARAMETERS FOR 2-D WAVE PROPAGATION PROBLEM WITH DIFFERENT CONTRAST RATIOS

Contrast Ratio		2	5	10	100
Time Step (s)		1.4e-10	4.9e-11	2.3e-11	2.3e-12
Num. of E	FDTD	220	1300	5100	501,000
	Subgridding	68	116	276	20256
Time (s)	FDTD	0.12	0.68	3.92	11237.47
	Subgridding	0.04	0.24	0.47	169.89
Speedup		3	2.83	8.34	66.14

For example, the analytical electric field at point $\mathbf{r}_i$ along the direction $\hat{t}_i$ should be $\mathbf{E}_{\text{inc}}(\mathbf{r}_i) \cdot \hat{t}_i$. It is clear to see that the simulated fields agree with the analytical solution very well. To examine the solution error in the entire computational domain, we calculate the relative error of the entire E unknown vector as $\|\{e\} - \{e\}_{\text{anal}}\|/\|\{e\}_{\text{anal}}\|$ at each time step with contrast ratio being 2, 5, 10, and 100, respectively. The entire solution error is shown in Fig. 4(c). Obviously, the solution accuracy in the entire computational domain is always very good for the four contrast ratios. The lower the contrast ratio is, the better the accuracy is. Meanwhile, the accuracy is saturated once the contrast ratio reaches a certain value.

In this example, we also examine the dispersion error of the proposed subgridding method. The same pulse is used. The electric field is sampled at the center point of the subgrid, which is then Fourier transformed. The ratio of the Fourier transformed response over the Fourier transform of the total field, which is also the incident field for this free-space example, is computed at the left boundary to extract the numerical phase velocity. This velocity compared with the ideal speed of light c is plotted as a function of frequency in Fig. 5. As can be seen, a good accuracy is observed in the entire working frequency band. In addition, as expected, the dispersion error at a higher grid ratio is shown to be greater than that at a lower grid ratio.

To demonstrate the efficiency of the proposed FDTD subgridding method, we also simulate the same problem using the conventional FDTD method with uniform fine grids. The simulation parameters are summarized in Table I. A significant CPU time speedup is observed from the proposed subgridding method as it uses many less unknowns than the conventional FDTD method.

B. 3-D Wave Propagation

The second example is a free-space wave propagation problem in a 3-D cube. The size of the computational domain in each direction is 5.1 m. Along all the directions, the coarse space step L_c is 0.1 m, resulting in 132 651 coarse cells. The coarse cell at the center is further subdivided into fine cells with contrast ratio being 5, and therefore, the fine grid size L_f is 0.02 m. The total number of E unknowns in the mesh is 414 240. The same incident field is supplied as that of the first example. An exact absorbing boundary condition is also supplied to all the unknowns on the boundary.

The existence of fine cells renders the time step of the proposed FDTD subgridding method less than 4.0×10^{-11} s. Since the analytical solution to this problem is known, we first plot the simulated electric field at two observation points in comparison with the analytical solution in Fig. 6(a).

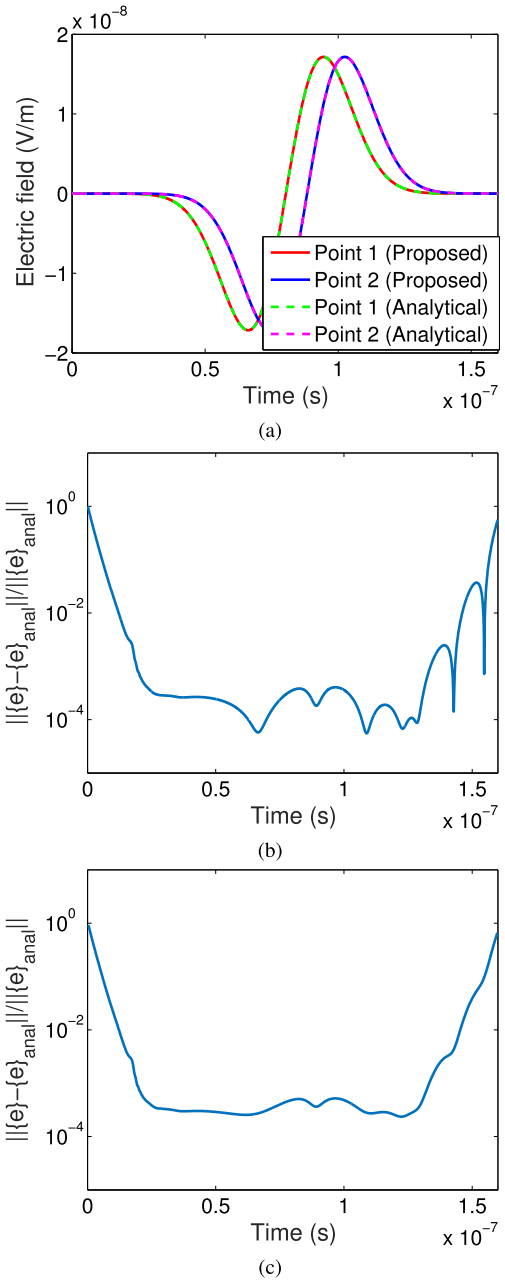

Fig. 6. Simulation of a 3-D wave propagation problem. (a) Simulated electric field at two observation points in comparison with reference analytical solutions. (b) Entire solution error versus time. (c) Entire solution error versus time when the unconditionally stable methods are applied to the proposed FDTD subgridding method.

Point 1 is at (0.1, 0.1, 0.05) m and it is inside the coarse mesh. The location of point 2 is (2.5, 2.5, 2.59) m and it is within the subgridding mesh. Obviously, the electric field waveforms at both points agree with the reference results very well. To examine the solution accuracy in the entire computational domain, in Fig. 6(b), we assess the entire solution error measured by $\|\{e\} - \{e\}_{\text{anal}}\|/\|\{e\}_{\text{anal}}\|$, where $\{e\}$ consists of all 414 240 $\mathbf{E}$ unknowns obtained from the proposed FDTD subgridding method, while $\{e\}_{\text{anal}}$ is from the analytical result. As can be seen clearly, the proposed method is accurate at all points and across the whole time window simulated. The larger errors at early and late time are because the denominator of the solution error is zero at those times.

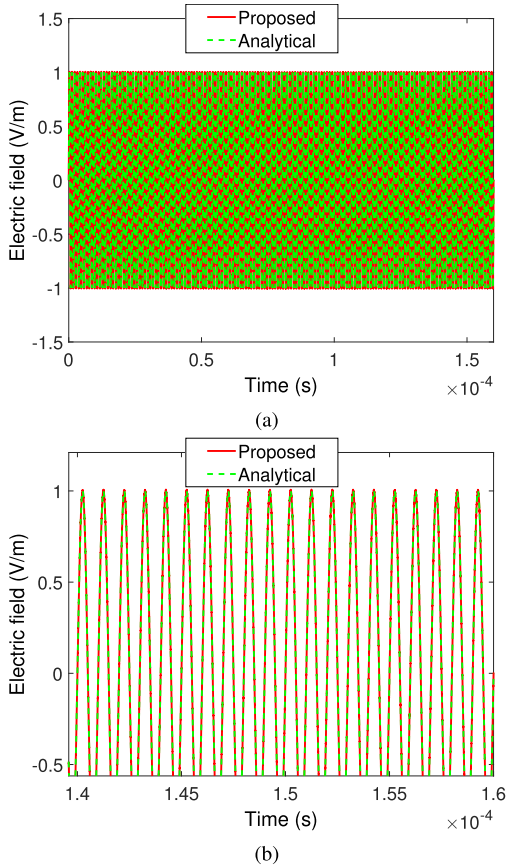

Fig. 7. Examination of late-time stability and accuracy of the subgridding method. (a) Overall plot. (b) Details.

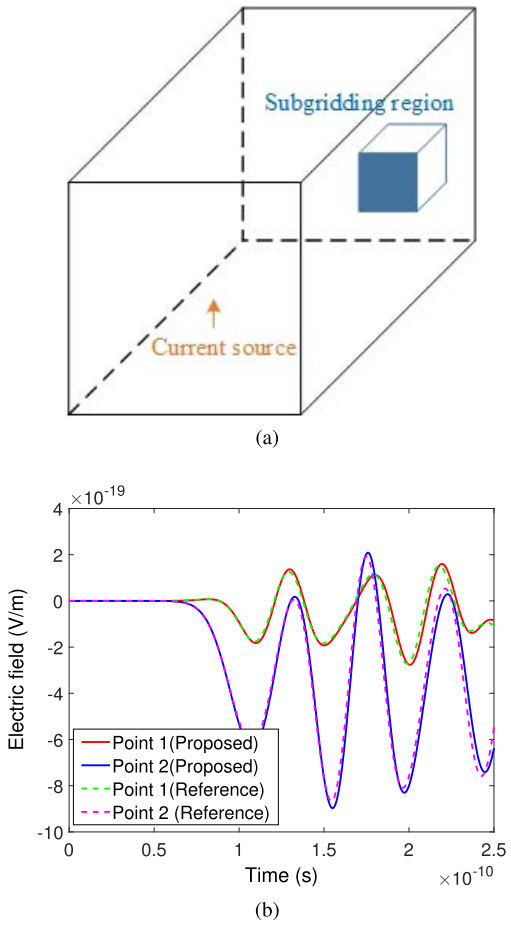

Fig. 8. Simulation of a 3-D cavity excited by a current source. (a) Structure details. (b) Simulated electric field at two observation points in comparison with reference FDTD solutions.

The proposed FDTD subgridding method takes 201.09 s to finish the simulation. To demonstrate the efficiency of the proposed method, we also discretize the same computational domain into uniform fine grids and simulate the same wave propagation problem in this domain using the conventional FDTD method. This uniform fine mesh involves 50 135 040 E unknowns. The times step is the same as that used in the proposed FDTD subgridding method, and it takes the conventional FDTD method 29012.74 s. Therefore, the proposed FDTD subgridding method is much faster than the conventional FDTD method when fine features exist. This is because the number of unknowns is reduced significantly.

We also simulated this example by using the proposed unconditionally stable FDTD subgridding method. First of all, the fine cells are identified, which involves 672 E unknowns and 552 H unknowns, and then, 320 unstable eigenmodes are extracted from $\mathbf{C}_f$ assembled from fine cells only. After the contribution of unstable eigenmodes is removed from the system matrix, we are allowed to use $\Delta t = 1.9\times10^{-10}$ s that is solely determined by accuracy for time marching. The entire solution error compared with the analytical solution at each time step is plotted in Fig. 6(c). It is evident that the accuracy is preserved by comparing Fig. 6(b) with Fig. 6(c). Since the proposed FDTD subgridding method can use a much larger time step after the unconditionally stable method is applied, it only takes 28.37 s to finish the simulation.

To investigate the late-time stability, we use a sinusoidal source and simulate the same problem for a very long time using the proposed unsymmetric subgridding method. The simulated electric field compared with the analytical solution is plotted in Fig. 7 as a function of time. A good accuracy is observed in the entire range, and no instability is observed. The numerical phase velocity is extracted and its ratio to the exact speed of light is found to be 1.0098.

C. 3-D Cavity With Current Probe Excitation

In this example, we simulate a 3-D cavity excited by a current source, as shown in Fig. 8(a). The cavity is 1 cm long in all directions and its six faces are all terminated by the PEC boundary condition. The coarse grid size along each direction is 1 mm except for the blue cube inside the cavity. The blue cube is centered at (4.5, 4.5, 4.5) mm and 1 mm long in all directions. It is filled with a conductive material whose conductivity is 5.7×10^7 S/m. The blue cube is further subdivided into fine mesh whose grid size is 0.2 mm, and therefore, the contrast ratio CR for this problem is 5. Such a subgridding mesh results in 4158 E unknowns. A current probe is excited at (2, 2, 1.5) mm. The current is a Gaussian pulse whose waveform is $\mathbf{I} = \hat{z}\exp-(t-t_0)^2/\tau^2$ with $\tau = 2\times10^{-11}$ s and $t_0 = 4\tau$. As the reference, we also simulate the same problem using the conventional FDTD method with a uniform fine mesh. The total number of E unknowns in this uniform fine mesh is 390 150. Since both

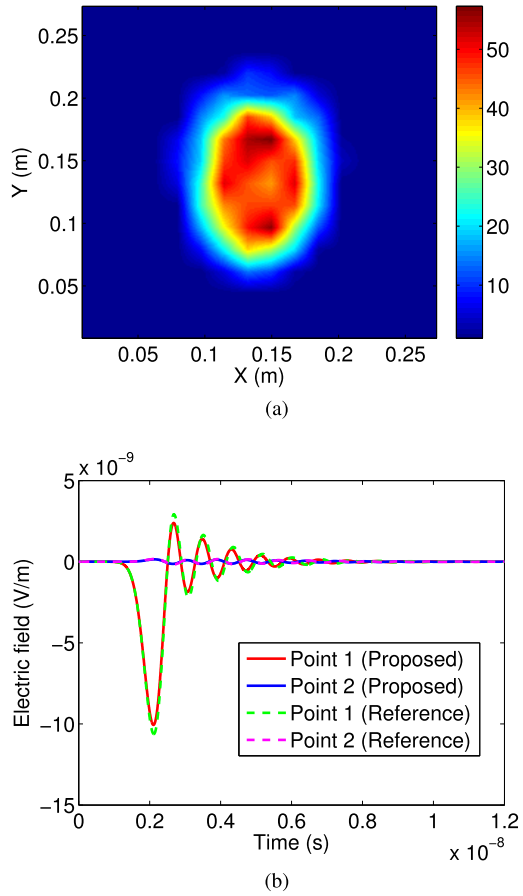

Fig. 9. Simulation of a phantom head beside a wire antenna. (a) Relative permittivity distribution in a cross section of the phantom head at z = 2.8 cm. (b) Simulated electric field at two observation points in comparison with reference FDTD solutions.

the subgridding mesh and the uniform fine mesh have fine grids, the proposed FDTD subgridding method employs the same time step as the conventional FDTD method, which is $\Delta t = 3.8 \times 10^{-13}$ s for comparison. In Fig. 8(b), the electric field sampled at point 1 (8, 8, 7.5) mm and point 2 (4, 4, 9.5) mm is plotted in comparison with the reference solution. Overall, the accuracy of the sampled E-field is very good. As for the CPU time, the proposed FDTD subgridding method only takes 0.13 s to finish the entire simulation, while the conventional FDTD method requires 38.68 s, and thus, a significant speedup is achieved.

D. Inhomogeneous 3-D Phantom Head Beside a Wire Antenna

The last example we study is a large-scale phantom head [21] beside a wire antenna, which involves many inhomogeneous materials. The size of the phantom head is 28.16 cm × 28.16 cm × 17.92 cm. The permittivity distribution of the head at $z = 2.8$ cm is shown in Fig. 9(a). All the boundaries are truncated by perfect magnetic conducting. The wire antenna is located at (3.52, 3.52, 2.52) cm, the current on which has a pulse waveform of $\mathbf{I} = 2(t - t_0)e^{-(t-t_0)^2/\tau^2}$ with $\tau = 5.0 \times 10^{-10}$ s and $t_0 = 4\tau$. The coarse step size along the x-, y-, and z-direction is 4.4, 4.4, and 5.6 mm, respectively. To capture fine tissues, two coarse cells at the center are subdivided into fine cells in all directions with contrast ratio $CR = 4$, meaning that the fine grid size along the x-, y-, and z-direction is 1.1, 1.1, and 1.4 mm, respectively. As a result, the total number of E unknowns in this subgridding mesh is 410 300. In the conventional FDTD, if fine grids are used everywhere, it would result in 25 428 608 E unknowns. Due to the existence of fine grids, both the proposed FDTD subgridding method and conventional FDTD method use a time step less than 2.2×10^{-12} s to ensure stability. In Fig. 9(b), the electric field at two observation points whose locations are (3.52, 3.52, 15.96) cm and (24.64, 3.52, 15.96) cm is plotted in comparison with reference solution that is obtained by simulating the same problem in a uniform fine grid using the conventional FDTD method. It is clear that the result from the proposed method agrees with the reference result. Since the conventional FDTD method requires a uniform find grid which has many more E unknowns than the proposed FDTD subgridding method, the conventional FDTD method takes 19222.16 s to finish the simulation.

The proposed unconditionally stable FDTD subgridding method is also used to simulate this example. To do so, the fine cells are first identified, which involve 724 electric field unknowns and 594 magnetic field unknowns. Given $\epsilon = 10^{-2}$, 325 unstable eigenmodes are obtained accurately from $\mathbf{S}_f$. With the unstable eigenmodes removed, the largest time step that can be used is increased from 2.2×10^{-12} s to 8.8×10^{-12} s, which is also the time step solely determined by accuracy. As a result, the unconditionally stable FDTD subgridding method only takes 159.23 s, including the time for extracting unstable eigenmodes and explicit time marching. However, without the unconditionally stable method, the FDTD subgridding method needs 528.53 s to finish the same simulation.

VII. Conclusion

In this paper, a novel unsymmetrical but stable FDTD subgridding algorithm is developed for a general electromagnetic analysis. We provide a theoretical analysis to show that the explicit FDTD time marching can be made stable if and only if all the eigenvalues of the governing system matrix are nonnegative real. This is satisfied by the original FDTD in a regular grid. However, in a subgridding algorithm, the original FDTD discretization of the curl operators has to be changed to ensure accuracy for field unknowns involved in the subgridding. This change usually results in an unsymmetrical system matrix supporting complex eigenvalues, and thus, the resulting explicit FDTD time marching becomes definitely unstable. Such an instability may not be observed at early time, but it will appear at late time. To resolve this problem, we propose a new time-marching scheme to stably simulate the unsymmetrical system, in which the system matrix has an explicit matrix inversion. As a result, the solution can also be obtained explicitly without running into the stability problem. This new time-marching scheme provides a flexibility to develop interpolation schemes solely based on the accuracy without concerning about the stability. It is also general for use, applicable to other subgridding algorithms. Essentially, this new scheme provides an effective means to explicitly simulate an unsymmetrical numerical system with guaranteed stability.

In addition, in this paper, an accurate subgridding algorithm is developed to generate the field unknowns on the subgrid interfaces for both 2-D and 3-D grids. The algorithm allows for an arbitrary grid contrast ratio. The time step allowed for an explicit time marching can be analytically found by analyzing the rank-1 matrices corresponding to the patches adjacent to the subgrid interface. This subgridding algorithm is then further made unconditionally stable. Extensive numerical experiments involving both 2- and 3-D subgrids with various contrast ratios have demonstrated the accuracy, stability, and efficiency of the proposed general method and new subgridding algorithm.

REFERENCES

[1] K. Yee, "Numerical solution of initial boundary value problems involving Maxwell's equations in isotropic media," *IEEE Trans. Antennas Propag.*, vol. 14, no. 3, pp. 302–307, May 1966.

[2] A. Taflove and S. C. Hagness, *Computational Electrodynamics*. Boston, MA, USA: Artech House, 2000.

[3] K. S. Kunz and L. Simpson, "A technique for increasing the resolution of finite-difference solutions of the Maxwell equation," *IEEE Trans. Electromagn. Compat.*, vol. TEMC-23, no. 4, pp. 419–422, Nov. 1981.

[4] S. S. Zivanovic, K. S. Yee, and K. K. Mei, "A subgridding method for the time-domain finite-difference method to solve Maxwell's equations," *IEEE Trans. Microw. Theory Techn.*, vol. 39, no. 3, pp. 471–479, Mar. 1991.

[5] D. T. Prescott and N. V. Shuley, "A method for incorporating different sized cells into the finite-difference time-domain analysis technique," *IEEE Microw. Guided Wave Lett.*, vol. 2, no. 11, pp. 434–436, Nov. 1992.

[6] M. J. White, M. F. Iskander, and Z. Huang, "Development of a multigrid FDTD code for three-dimensional applications," *IEEE Trans. Antennas Propag.*, vol. 45, no. 10, pp. 1512–1517, Oct. 1997.

[7] M. W. Chevalier, R. J. Luebbers, and V. P. Cable, "FDTD local grid with material traverse," *IEEE Trans. Antennas Propag.*, vol. 45, no. 3, pp. 411–421, Mar. 1997.

[8] M. J. White, Z. Yun, and M. F. Iskander, "A new 3D FDTD multigrid technique with dielectric traverse capabilities," *IEEE Trans. Microw. Theory Techn.*, vol. 49, no. 3, pp. 422–430, Mar. 2001.

[9] M. Okoniewski, E. Okoniewska, and M. A. Stuchly, "Three-dimensional subgridding algorithm for FDTD," *IEEE Trans. Antennas Propag.*, vol. 45, no. 3, pp. 422–429, Mar. 1997.

[10] K. Xiao, D. J. Pommerenke, and J. L. Drewniak, "A three-dimensional FDTD subgridding algorithm with separated temporal and spatial interfaces and related stability analysis," *IEEE Trans. Antennas Propag.*, vol. 55, no. 7, pp. 1981–1990, Jul. 2007.

[11] P. Thoma and T. Weiland, "A consistent subgridding scheme for the finite difference time domain method," *Int. J. Numer. Model., Electron. Netw., Devices Fields*, vol. 9, no. 5, pp. 359–374, Sep. 1996.

[12] O. Podebrad, M. Clemens, and T. Weiland, "New flexible subgridding scheme for the finite integration technique," *IEEE Trans. Magn.*, vol. 39, no. 3, pp. 1662–1665, May 2003.

[13] N. V. Venkatarayalu, R. Lee, Y. B. Gan, and L. W. Li, "A stable FDTD subgridding method based on finite element formulation with hanging variables," *IEEE Trans. Antennas Propag.*, vol. 55, no. 3, pp. 907–915, Mar. 2007.

[14] K. M. Krishnaiah and C. J. Railton, "A stable subgridding algorithm and its application to eigenvalue problems," *IEEE Trans. Microw. Theory Techn.*, vol. 47, no. 5, pp. 620–628, May 1999.

[15] J. Yan and D. Jiao, "Explicit and unconditionally stable FDTD method without eigenvalue solutions," in *IEEE MTT-S Int. Microw. Symp. Dig.*, May 2016, pp. 1–4.

[16] J. Yan and D. Jiao, "Fast explicit and unconditionally stable FDTD method for electromagnetic analysis," *IEEE Trans. Microw. Theory Techn.*, vol. 65, no. 8, pp. 2698–2710, Aug. 2017.

[17] J. Yan and D. Jiao, "Symmetric positive semidefinite FDTD subgridding algorithms for arbitrary grid ratios without compromising accuracy," *IEEE Trans. Microw. Theory Techn.*, vol. 65, no. 12, pp. 5084–5095, Dec. 2017.

[18] M. Gaffar and D. Jiao, "An explicit and unconditionally stable FDTD method for the analysis of general 3-D lossy problems," *IEEE Trans. Antennas Propag.*, vol. 63, no. 9, pp. 4003–4015, Sep. 2015.

[19] J. Yan and D. Jiao, "Accurate and stable matrix-free time-domain method in 3-D unstructured meshes for general electromagnetic analysis," *IEEE Trans. Microw. Theory Techn.*, vol. 63, no. 12, pp. 4201–4214, Dec. 2015.

[20] M. Gaffar and D. Jiao, "Alternative method for making explicit FDTD unconditionally stable," *IEEE Trans. Microw. Theory Techn.*, vol. 63, no. 12, pp. 4215–4224, Dec. 2015.

[21] I. G. Zubal, C. R. Harrell, E. O. Smith, Z. Rattner, G. Gindi, and P. B. Hoffer, "Computerized three-dimensional segmented human anatomy," *Med. Phys.*, vol. 21, no. 2, pp. 299–302, 1994.

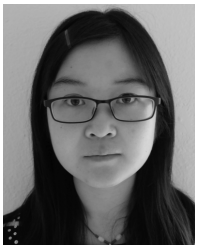

Jin Yan (S'13–M'17) received the B.S. degree in electronic engineering and information science from the University of Science and Technology of China, Hefei, China, in 2012, and the Ph.D. degree in electrical engineering from Purdue University, West Lafayette, IN, USA, in 2016.

She has been a Software Engineer with the Platform Engineering Group, Intel Corporation, Hillsboro, OR, USA, since 2016. Her current research interests include signal and power integrity, computational electromagnetics, high-performance very-large-scale integration CAD, and fast and high-capacity numerical methods.

Dr. Yan was a recipient of the Honorable Mention Award from the IEEE International Symposium on Antennas and Propagation in 2015 and the Best Student Paper Award Finalist from the IEEE MTT-S International Microwave Symposium in 2016.

Dan Jiao (M'02–SM'06–F'16) received the Ph.D. degree in electrical engineering from the University of Illinois at Urbana–Champaign, Champaign, IL, USA, in 2001.

She was with the Technology Computer-Aided Design (CAD) Division, Intel Corporation, Santa Clara, CA, USA, until 2005, as a Senior CAD Engineer, a Staff Engineer, and a Senior Staff Engineer. In 2005, she joined the School of Electrical and Computer Engineering, Purdue University, West Lafayette, IN, USA, as an Assistant Professor, where she is currently a Professor. She has authored three book chapters and over 260 papers in refereed journals and international conferences. Her current research interests include computational electromagnetics, high-frequency digital, analog, mixed-signal, RF integrated circuit design and analysis, high-performance very-large-scale integration CAD, modeling of microscale and nanoscale circuits, applied electromagnetics, fast and high-capacity numerical methods, fast time-domain analysis, scattering and antenna analysis, RF, microwave, millimeter-wave circuits, wireless communication, and bioelectromagnetics.

Dr. Jiao was a recipient of the 2000 Raj Mittra Outstanding Research Award, presented by the University of Illinois at Urbana–Champaign, the Intel Corporation LTD Team Quality Award, the 2002 Intel Corporation Components Research the Intel Hero Award (Intel-wide she was the tenth recipient), the 2003 Intel Corporation Logic Technology Development (LTD) Divisional Achievement Award, the Intel Corporation Technology CAD Divisional Achievement Award, the 2010 Ruth and Joel Spira Outstanding Teaching Award, the 2004 Best Paper Award presented at the Intel Corporation annual corporate-wide technology conference (Design and Test Technology Conference) for her work on generic broadband model of high-speed circuits, the 2006 Jack and Cathie Kozik Faculty Start up Award (which recognizes an outstanding new faculty member of the School of Electrical and Computer Engineering, Purdue University), the 2006 Office of Naval Research Award under the Young Investigator Program, the 2008 National Science Foundation CAREER Award, and the 2013 S. A. Schelkunoff Prize Paper Award from the IEEE Antennas and Propagation Society, which recognizes the best paper published in the IEEE TRANSACTIONS ON ANTENNAS AND PROPAGATION during the previous year. She was among the 21 women faculty selected across the country as the 2014–2015 Fellow of Executive Leadership in Academic Technology and Engineering at Drexel, a national leadership program for women in the academic STEM fields. She was among the 85 engineers selected throughout the nation for the National Academy of Engineering 2011 U.S. Frontiers of Engineering Symposium. She has been named a University Faculty Scholar by Purdue University since 2013. She is an Associate Editor of the IEEE Transactions on Components, Packaging, and Manufacturing Technology. She has served as a reviewer for many IEEE journals and conferences.